

# Impact of nuclear dependence of $R = \sigma_L/\sigma_T$ on antishadowing in nuclear structure functions

Vadim Guzey,<sup>1</sup> Lingyan Zhu,<sup>1</sup> Cynthia E. Keppel,<sup>1</sup> M. Eric Christy,<sup>1</sup> Dave Gaskell,<sup>2</sup> Patricia Solvignon,<sup>2</sup> and Alberto Accardi<sup>1,2</sup>

<sup>1</sup>Hampton University, Hampton, VA 23668, USA

<sup>2</sup>Thomas Jefferson National Accelerator Facility, Newport News, VA 23606, USA

(Dated: October 24, 2018)

We study the impact of the nuclear dependence of  $R = \sigma_L/\sigma_T$  on the extraction of the  $F_2^A/F_2^D$  and  $F_1^A/F_1^D$  structure function ratios from the data on the  $\sigma^A/\sigma^D$  cross section ratios. Guided by indications of the nuclear dependence of  $R$  from the world data, we examine selected sets of EMC, BCDMS, NMC and SLAC data and find that  $F_1^A/F_1^D < \sigma^A/\sigma^D \leq F_2^A/F_2^D$ . In particular, we observe that the nuclear enhancement (antishadowing) for  $F_1^A/F_1^D$  in the interval  $0.1 < x < 0.3$  becomes significantly reduced or even disappears, which indicates that antishadowing is dominated by the longitudinal structure function  $F_L$ . We also argue that precise measurements of nuclear modifications of  $R$  and  $F_L^A$  have the potential to constrain the poorly known gluon distribution in nuclei over a wide range of  $x$ .

## 1. INTRODUCTION

Since the early lepton scattering experiments that discovered the substructure of the nucleon and eventually led to the development of Quantum Chromodynamics (QCD) as the theory of the strong interaction, deep inelastic scattering (DIS) has been a critical tool in the investigation of the quark and gluon structure of nucleons and nuclei. While initially nuclear effects in DIS were thought to be largely negligible, this was proven wrong by the measurement of the ratio of the iron to deuterium structure functions performed by the European Muon Collaboration (EMC) at CERN in 1983 [1]. The apparent disagreement between the dramatic deviation of the ratio from unity seen in the EMC data and the small nuclear effects predicted by theoretical calculations has triggered a series of further measurements and theoretical investigations, for reviews, see [2–5].

The emerging picture of nuclear modifications of the nucleus to deuteron cross section ratio,  $\sigma^A/\sigma^D$ , has the pattern presented in Fig. 1. For small values of Bjorken  $x$ ,  $x < 0.05 - 0.1$ , the ratio is noticeably suppressed—the suppression increases with an increase of the atomic number  $A$  and a decrease of  $x$ —which is called nuclear shadowing. For  $0.1 < x < 0.3$ , the ratio is enhanced; the effect is small (of the order of a few percent) and does not reveal an obvious  $A$  dependence. In the interval  $0.3 < x < 0.8$ , the ratio is suppressed and this suppression is called the EMC effect. Finally, for  $x > 0.8$  the ratio dramatically grows above unity which is explained by the effect of the nucleon motion inside nuclei (Fermi motion). Various models describe the experimental  $\sigma^A/\sigma^D$  cross section ratios for certain ranges of Bjorken  $x$ , but there is no comprehensive understanding of the entire pattern of the nuclear modifications described above. In particular, there is no unique and generally accepted theory to explain the nature of the antishadowing and EMC effects.

In this paper we focus on the enhancement (antishad-

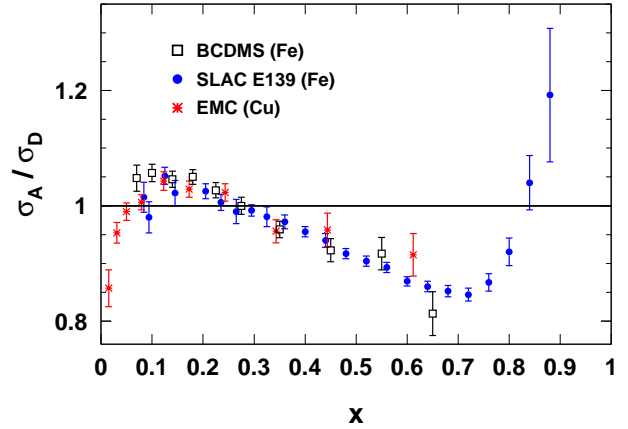


FIG. 1: The pattern of nuclear modifications of the  $\sigma^A/\sigma^D$  cross section ratio as a function of Bjorken  $x$  for  $^{56}\text{Fe}$  and  $^{64}\text{Cu}$ . The data are from BCDMS [6] (open squares), SLAC E139 [7] (filled circles) and EMC [8] (stars). For all data sets statistical and systematic errors have been combined in quadrature.

owing) of the  $\sigma^A/\sigma^D$  cross section ratios in the  $0.1 < x < 0.3$  region. The deviation of  $\sigma^A/\sigma^D$  from unity in the antishadowing region is of the order of a few percent [2–5] (see Fig. 1). Given that most measurements quote normalization uncertainties on the order of 1-2% (usually due to target thickness or luminosity), it is difficult to quantify the absolute size of the antishadowing effect precisely, and comparisons between experiments are somewhat complicated. In addition, systematic uncertainties due to radiative corrections are highly non-trivial in this region of  $x$ , and are sometimes hard to determine accurately. An example of the difficulty involved in achieving very precise measurements in the antishadowing region can be found in the SLAC E139 results. The preliminary

results for the Fe/D ratio were essentially consistent with unity for the region  $0.1 < x < 0.3$  [9]. However, the final E139 analysis yielded results in the antishadowing region more consistent with, e.g., the EMC and BCDMS experiments, showing a small enhancement of  $\approx 3\%$  on average [7]. Despite the difficulties inherent in antishadowing measurements, the results from various experiments are remarkably consistent within their experimental uncertainties. In addition, the small enhancement seen by the EMC, BCDMS, and SLAC E139 experiments for copper and iron targets has also been seen in lighter targets (Ca/D, N/D, C/D, He/D) by the NMC [10] and HERMES [11] experiments.

The antishadowing effect has rather intriguing features. Unlike the shadowing effect, antishadowing showed little or no sensitivity to the mass number  $A$  within experimental uncertainties, for example, in the SLAC E139 [7] and NMC data [10]. While antishadowing is observed in nuclear DIS, the cross section enhancement is not seen in nuclear Drell-Yan rates [12] and total neutrino-nucleus cross sections for  $x > 0.1$  [13].

In the leading twist formalism, the small enhancement of  $\sigma^A/\sigma^D$  in the antishadowing region translates into an enhancement of the valence quark and possibly gluon distributions in nuclei in this region [13–17]. However, the pattern and especially the magnitude of nuclear modifications of the gluon distribution in nuclei are very poorly constrained by present data.

The aim of this paper is to examine the impact of the nuclear dependence of  $R = \sigma_L/\sigma_T$ , i.e., the ratio of the longitudinal to transverse photoabsorption cross sections, on the extraction of the nucleus to deuteron structure function ratios,  $F_2^A/F_2^D$  and  $F_1^A/F_1^D$ , from  $\sigma^A/\sigma^D$  data. In particular, we demonstrate that in the presence of a small but non-zero difference between  $R$  for nuclei and the nucleon, the nuclear enhancement in the ratio of the transverse structure functions  $F_1^A/F_1^D$  becomes significantly reduced (or even disappears in some cases), indicating that antishadowing is dominated by the longitudinal contribution. In addition, we analyze how the nuclear dependence of  $R$  affects the nuclear gluon distribution and emphasize the importance of measurements of  $R$  in the DIS kinematics as a direct probe of the gluon distribution in nuclei.

## 2. NUCLEAR DEPENDENCE OF $R$ AND THE RATIO OF NUCLEUS AND DEUTERON STRUCTURE FUNCTIONS

### 2.1. Longitudinal contribution to the inclusive cross section

In the one-photon exchange approximation, the spin-independent cross section for inclusive electron scattering can be expressed as

$$\frac{d^2\sigma}{d\Omega dE'} = \Gamma [\sigma_T(x, Q^2) + \epsilon\sigma_L(x, Q^2)]$$

$$= \Gamma\sigma_T(x, Q^2) [1 + \epsilon R(x, Q^2)], \quad (1)$$

where  $\sigma_T$  ( $\sigma_L$ ) is the cross section for photoabsorption of purely transversely (longitudinally) polarized photons;  $R = \sigma_L/\sigma_T$ ;  $\Gamma$  is the transverse virtual photon flux;  $\epsilon$  is the virtual photon polarization parameter. In the laboratory frame, the negative four-momentum squared (virtuality) of the exchanged photon is  $-q^2 = Q^2 = 4EE'\sin^2(\theta/2)$  and the Bjorken  $x$  is  $x = Q^2/[2M(E - E')]$ , where  $E$  ( $E'$ ) is the energy of the incident (scattered) electron,  $\theta$  is the scattering angle, and  $M$  is the nucleon mass. The flux of transverse virtual photons can be expressed as  $\Gamma = \alpha E'(W^2 - M^2)/[4\pi^2 Q^2 M E(1 - \epsilon)]$ , where  $\alpha$  is the fine structure constant and  $W$  is the invariant energy of the virtual photon-proton system. Finally, the virtual photon polarization parameter is:

$$\begin{aligned} \epsilon &= \left[ 1 + 2\left(1 + \frac{\nu^2}{Q^2}\right)\tan^2\frac{\theta}{2} \right]^{-1} \\ &= \frac{1 - y - \frac{M^2 x^2 y^2}{Q^2}}{1 - y + \frac{y^2}{2} + \frac{M^2 x^2 y^2}{Q^2}}. \end{aligned} \quad (2)$$

where  $\nu = E - E'$ ;  $y = \nu/E$ . Note that in the second line of Eq. (2) we expressed  $\epsilon$  in a Lorentz invariant form.

In terms of the structure functions  $F_1(x, Q^2)$  and  $F_2(x, Q^2)$  in the DIS region, the double differential cross section can be written as

$$\begin{aligned} \frac{d^2\sigma}{d\Omega dE'} &= \Gamma \frac{4\pi^2\alpha}{x(W^2 - M^2)} \\ &\times \left[ 2xF_1 + \epsilon \left( \left(1 + \frac{4M^2 x^2}{Q^2}\right)F_2 - 2xF_1 \right) \right]. \end{aligned} \quad (3)$$

A comparison of Eqs. (1) and (3) shows that  $F_1(x, Q^2)$  is purely transverse, while

$$F_L(x, Q^2) = \left(1 + \frac{4M^2 x^2}{Q^2}\right)F_2(x, Q^2) - 2xF_1(x, Q^2) \quad (4)$$

is purely longitudinal. Note that  $F_2(x, Q^2)$  is a mixture of both the longitudinal and transverse contributions. Thus, the ratio  $R$  is

$$R \equiv \frac{\sigma_L}{\sigma_T} = \frac{F_L(x, Q^2)}{2xF_1(x, Q^2)}. \quad (5)$$

The nucleon structure function  $F_2(x, Q^2)$  is proportional to the  $d^2\sigma/(d\Omega dE')$  differential cross section in the  $\epsilon \rightarrow 1$  limit; it has been measured with high precision in various  $x$  and  $Q^2$  bins. The longitudinal structure function  $F_L(x, Q^2)$ , in contrast, is not measured as well as  $F_2(x, Q^2)$ : the data is sparse and imprecise for the proton and is even more limited for nuclei. It is an experimental challenge to separate  $F_2(x, Q^2)$  and  $F_L(x, Q^2)$  which is usually done using the method of Rosenbluth separation, i.e., by measuring the cross section at different energies (at fixed  $x$  and  $Q^2$ ) to allow for a variation of  $\epsilon$ .

In this paper we shall use the parameterization of  $R$  for the nucleon,  $R^N$ , that was obtained as the result of the global analysis of the SLAC hydrogen and deuterium data [18]. The same analysis also showed that  $R^D = R^H$  to high accuracy, where  $R^D$  ( $R^H$ ) refers to deuterium (hydrogen). An example of the values of  $R^N$  in the kinematics used in this paper is presented in the middle panel of Fig. 2. Note that the more recent analysis of the SLAC E143 collaboration [19] reported results for  $R^N$  consistent with those of Ref. [18].

## 2.2. Hints of nontrivial nuclear dependence of $R$

Experimentally measured cross section ratios contain both transverse and longitudinal contributions of the structure functions. In terms of the structure function  $F_2(x, Q^2)$ , one can write the ratio of the nucleus to deuteron photoabsorption cross sections as

$$\begin{aligned} \frac{\sigma^A}{\sigma^D} &= \frac{F_2^A(x, Q^2)}{F_2^D(x, Q^2)} \frac{1 + R^D}{1 + R^A} \frac{1 + \epsilon R^A}{1 + \epsilon R^D} \\ &\approx \frac{F_2^A(x, Q^2)}{F_2^D(x, Q^2)} \left[ 1 - \frac{\Delta R(1 - \epsilon)}{(1 + R^D)(1 + \epsilon R^D)} \right], \quad (6) \end{aligned}$$

where the superscript  $A$  refers to the nucleus and the superscript  $D$  refers to the deuteron;  $\Delta R \equiv R^A - R^D$ . In the second line of Eq. (6) we used the expansion in terms of the small parameter  $\Delta R$  and kept first two terms of the expansion.

Alternatively one can express the cross sections  $\sigma^A$  and  $\sigma^D$  in terms of the structure function  $F_1(x, Q^2)$  and obtain:

$$\begin{aligned} \frac{\sigma^A}{\sigma^D} &= \frac{F_1^A(x, Q^2)}{F_1^D(x, Q^2)} \frac{1 + \epsilon R^A}{1 + \epsilon R^D} \\ &= \frac{F_1^A(x, Q^2)}{F_1^D(x, Q^2)} \left[ 1 + \frac{\epsilon \Delta R}{1 + \epsilon R^D} \right]. \quad (7) \end{aligned}$$

The cross section ratio  $\sigma^A/\sigma^D$  can be identified with the structure function ratio  $F_2^A/F_2^D$  or  $F_1^A/F_1^D$  only with the assumption of the trivial nuclear dependence of  $R = \sigma_L/\sigma_T$ , i.e.,  $R^A = R^D$ , or in certain kinematic limits. In particular,  $\sigma^A/\sigma^D = F_2^A/F_2^D$  at  $\epsilon = 1$  and  $\sigma^A/\sigma^D = F_1^A/F_1^D$  at  $\epsilon = 0$ .

Figure 2 presents the kinematic coverage in  $Q^2$  and  $x$  and the corresponding values of  $\epsilon$  and  $R^N$  of the data points considered in this paper. On the one hand, the BCDMS [6], EMC [8] and NMC [10] data are mostly taken with  $\epsilon$  close to unity (see the upper panel of Fig. 2), which implies that the cross section ratios are close to the  $F_2$  structure function ratios, even if  $\Delta R \equiv R^A - R^D \neq 0$ . On the other hand, the SLAC data [7, 20] (see the upper panel of Fig. 2) corresponds to the kinematics where  $\epsilon \approx 0.5$  and, hence,  $F_2^A/F_2^D$  will deviate from  $\sigma^A/\sigma^D$  if  $\Delta R \neq 0$ . For all these experiments  $\epsilon \neq 0$  and, hence, the extraction of the transverse structure function ratios  $F_1^A/F_1^D$  depends explicitly on the assumption adopted

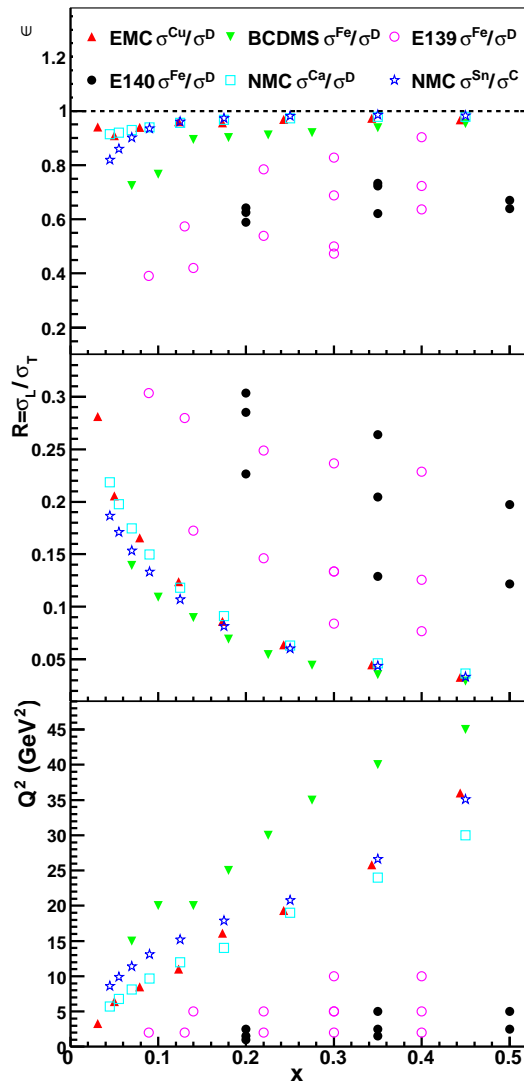


FIG. 2: The kinematic coverage in  $Q^2$  and  $x$  and the corresponding values of  $\epsilon$  and  $R^N$  of the data points considered in this paper.

for  $\Delta R$ . Below we summarize what is known about it from the world data.

At small  $Q^2$ ,  $R$  might be different between deuterium and hydrogen [21], though it seems to be identical at large  $Q^2$  [22, 23]. In particular, there are some hints in both JLab E99-118 [21] and SLAC data [23] that  $R^D$  is smaller than  $R^H$  for  $Q^2 < 1.5$  GeV<sup>2</sup>, with a global average of  $R^D - R^H = -0.054 \pm 0.029$ .

Turning to heavier nuclei, the SLAC E140 data [20] suggest some nuclear dependence of  $R$  at  $x = 0.2$ , which seems to have a nontrivial  $Q^2$  dependence:  $R^{Fe} - R^D$  can be positive at  $Q^2 = 2.5$  GeV<sup>2</sup> and negative at  $Q^2 = 1.5$  and 1 GeV<sup>2</sup>:

$$\begin{aligned} R^{Fe} - R^D|_{Q^2=2.5} &= 0.144 \pm 0.079(\text{stat.}) \pm 0.027(\text{syst.}); \\ R^{Fe} - R^D|_{Q^2=1.5} &= -0.124 \pm 0.051(\text{stat.}) \pm 0.023(\text{syst.}); \\ R^{Fe} - R^D|_{Q^2=1} &= -0.086 \pm 0.057(\text{stat.}) \pm 0.022(\text{syst.}). \end{aligned}$$

A word of caution is in order here. Coulomb corrections may be non-negligible in DIS at SLAC and JLab kinematics, especially at large  $x$ . These corrections tend to reduce  $R$  for nuclear targets [24].

The nuclear dependence of  $R$  at  $Q^2$  of the order of a few  $\text{GeV}^2$  and lower was also measured by the HERMES collaboration [11] by fitting the  $\sigma^A/\sigma^D$  cross section as a function of the virtual photon polarization  $\epsilon$  over a typical range of  $0.4 < \epsilon < 0.7$ . Overall no significant nuclear dependence of  $R$  for  $^{14}\text{N}$  and  $^3\text{He}$  targets for  $x > 0.06$  has been observed (the data in the  $x < 0.06$  region is affected by the correlated background and should be neglected). However, since this was a single-energy measurement with correlated values of  $\epsilon$  and  $Q^2$ , the extraction of  $R^A/R^D$  was done in a model-dependent way.

At larger values of  $Q^2$ , the NMC experiment [25] obtained  $R^{Ca} - R^C = 0.027 \pm 0.026(\text{stat.}) \pm 0.020(\text{syst.})$  at  $\langle Q^2 \rangle = 4 \text{ GeV}^2$  and concluded that  $\Delta R$  is compatible with zero. However, a hint of the nontrivial nuclear dependence of  $R$  can be still seen in data. The precision Sn/C data from NMC [26] show that  $R^{Sn} - R^C = 0.040 \pm 0.021(\text{stat.}) \pm 0.026(\text{syst.})$  at a mean  $Q^2$  of  $10 \text{ GeV}^2$ . This value of  $\Delta R \equiv R^A - R^D$  corresponds to  $\Delta R/R^N = 0.22 \div 1.20$ , i.e., 22 – 120 % relative deviation for different values of  $x$  in the considered kinematics, where  $R^N$  is given by the parameterization of Ref. [18] presented in the middle panel of Fig. 2. Note that the extraction of  $\Delta R$  in this experiment was based on a method closely related to Rosenbluth separation taking advantage of three different incident muon energies (120, 200 and 280 GeV).

For convenience, we present in Table I a brief overview (covered kinematics in Bjorken  $x$  and  $Q^2$  and energy settings) of the discussed measurements of the nuclear dependence of  $R$  (involving nuclei heavier than deuterium).

Experiment and observables	Kinematics	Beam energy
SLAC E140 [20] $R^{Fe,Au} - R^D$	$0.2 \leq x \leq 0.5$ $1 \leq Q^2 \leq 10 \text{ GeV}^2$	$3.7 \leq E \leq 15 \text{ GeV}$ , up to five energies
NMC (1992) [25] $R^{Ca} - R^C$	$0.0085 \leq x \leq 0.15$ $1 \leq Q^2 \leq 15 \text{ GeV}^2$	$E = 90$ and $200 \text{ GeV}$ , two energies
HERMES [11] $R^{^3He,Ne}/R^D$	$0.01 < x < 0.8$ $0.2 < Q^2 < 3 \text{ GeV}^2$	$E = 27.5 \text{ GeV}$ single energy
NMC (1996) [26] $R^{Sn} - R^C$	$0.0125 \leq x \leq 0.45$ $3.3 \leq Q^2 \leq 35 \text{ GeV}^2$	$E = 120, 200, 280$ GeV, three energies

TABLE I: An overview of the measurements of the nuclear dependence of  $R$  discussed in this paper.

The results of the NMC measurement of  $R^{Sn} - R^C$  as a function of Bjorken  $x$  [26] are presented as full squares in Fig. 3. For completeness, we also show the NMC result for the average  $R^{Ca} - R^C$  [25] as a triangle, the SLAC E140 result for the average  $R^{Au} - R^{Fe}$  [27] as an inverse triangle, and the SLAC E140 results for  $R^{Fe} - R^D$  as a function of  $x$  [20] as open circles. (For the latter, we showed only the data points for the 6% radiation

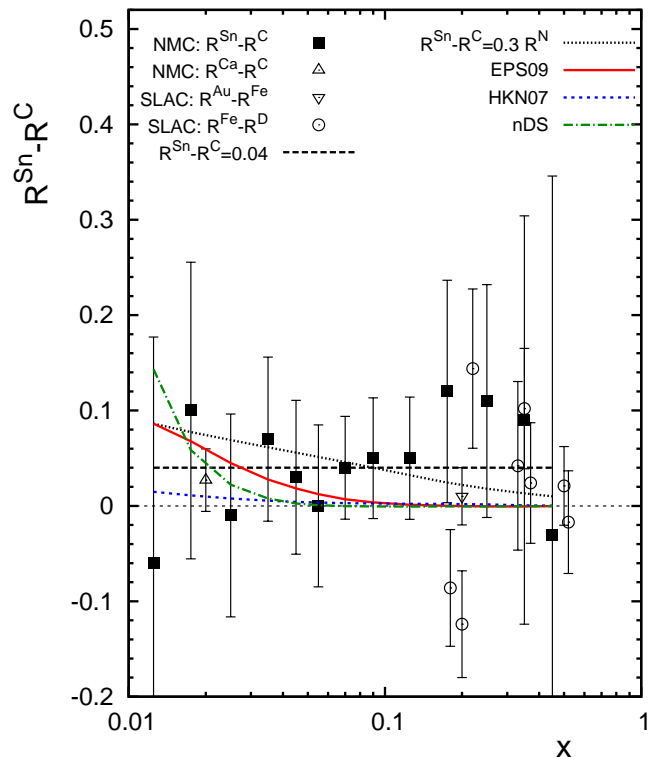


FIG. 3:  $R^{Sn} - R^C$  as a function of  $x$ . Full squares are results of the NMC measurement with the statistical and systematic errors added in quadrature [26]; the long-dash and dotted curves correspond to  $R^{Sn} - R^C = 0.04$  and  $R^{Sn} - R^C = 0.3R^N$ , respectively; the curves labeled “EPS09”, “HKN07” and “nDS” correspond to predictions using different nuclear parton distributions. Also shown are the NMC result for  $R^{Ca} - R^C$  [25] (triangle), the SLAC result for  $R^{Au} - R^{Fe}$  [27] (inverse triangle), and SLAC E140 results for  $R^{Fe} - R^D$  as a function of  $x$  [20] (open circles).

length iron target and shifted them in  $x$  for better visibility.) The long-dash and dotted curves correspond to  $R^{Sn} - R^C = 0.04$  and  $R^{Sn} - R^C = 0.3R^N$ , respectively. As one can see from the figure, both curves provide a good description of the measured values of  $R^{Sn} - R^C$ . Finally, the curves labeled “EPS09”, “HKN07” and “nDS” correspond to the direct calculation of  $R^{Sn} - R^C$  using different parameterizations of leading twist nuclear parton distributions (PDFs), see the discussion in Sect. 4. Note that we have singled out the NMC Sn/C data [26] because the extraction of  $R^A - R^D$  was done using a method closely related to the Rosenbluth separation and because the covered kinematics (the values of  $x$ ,  $Q^2$  and  $\epsilon$ ) broadly overlaps with that of the BCDMS, EMC, and NMC data on  $\sigma^A/\sigma^D$  that we analyze in this paper.

In summary, as a global average, while  $R$  seems to show little nuclear dependence within relatively large experimental uncertainties, there exist hints of nontrivial nuclear dependence of  $R$ . In particular,  $\Delta R = R^A - R^D$  may be statistically different from zero in some kinemat-

ics.

### 2.3. Impact of nuclear dependence of $R$ on nucleus to deuteron structure function ratios

As we explained in Sect. 2.2, if there is a nontrivial nuclear dependence of  $R$ , the  $\sigma^A/\sigma^D$  cross section ratio is not equal to the  $F_1^A/F_1^D$  or  $F_2^A/F_2^D$  structure ratios. In particular, a positive  $R^A - R^D$  will lead to  $F_1^A/F_1^D < \sigma^A/\sigma^D < F_2^A/F_2^D$ . Since the nuclear dependence of  $R$  has not as yet been systematically measured, we shall test two assumptions for  $\Delta R$  that are motivated purely by the NMC Sn/C data [26], which has kinematic coverage similar to that of the BCDMS, EMC and NMC measurements. In our analysis below we assume that:

1) (Absolute)  $\Delta R = R^A - R^D = 0.04$ . This is based on the NMC measurement of  $R^{Sn} - R^C$  at an average  $\langle Q^2 \rangle = 10 \text{ GeV}^2$ .

2) (Relative)  $(R^A - R^D)/R^N = 30\%$ , which is possible in view of the fact that the NMC Sn/C data allows for the 22 – 120% relative deviation of  $\Delta R/R^N$ .

Note that we effectively assumed that  $R^A - R^D \approx R^{Sn} - R^C$  which corresponds to the lower limit for  $\Delta R$ .

The impact of our assumptions for  $\Delta R$  on selected nuclear DIS data is presented in Figs. 4 and 5, we truncated the used data sets by neglecting low  $x$  and high  $x$  data points and focusing on the antishadowing region.

The BCDMS Fe/D [6], EMC Cu/D [8] and NMC Ca/D [10] data presented in Fig. 4 correspond to  $\epsilon$  close to unity. Therefore, regardless of the assumption for  $\Delta R$ , one expects that  $F_2^A/F_2^D \approx \sigma^A/\sigma^D$  with a very good accuracy. On the other hand,  $F_1^A/F_1^D$  is clearly smaller than  $\sigma^A/\sigma^D$ . Thus, the few percent enhancement of  $\sigma^A/\sigma^D$  in the antishadowing region may be reduced or removed altogether for the ratio of the transverse structure functions  $F_1^A/F_1^D$ .

For the SLAC E139 [7] and E140 [20] Fe/D data presented in Fig. 5, the values of  $Q^2$  are rather small (see the lower panel in Fig. 2) and our assumptions for the nuclear dependence of  $R$  motivated by the NMC Sn/C measurement at higher  $Q^2$  require a significant extrapolation in  $Q^2$ . However, for the lack of better input, in our analysis of the SLAC data we adopt the same assumptions for  $\Delta R$  as those used above. Since the values of  $\epsilon$  for these two data sets are not close to unity (see the upper panel in Fig. 2),  $\Delta R > 0$  leads to noticeable differences between the ratio of the structure functions and the ratio of the cross sections according to the trend described by Eqs. (6) and (7):  $F_1^A/F_1^D < \sigma^A/\sigma^D < F_2^A/F_2^D$ .

In summary, the assumed nontrivial nuclear dependence of  $R$  leads to a decrease or to a complete disappearance (in some case) of enhancement of the  $F_1^A/F_1^D$  structure function ratio in the  $0.1 < x < 0.3$  region. If confirmed by future experiments, this observation would indicate that the effect of antishadowing in  $\sigma^A$  is predominantly due to the contribution of the longitudinal structure function  $F_L^A$ , instead of  $F_1^A$  as implicitly as-

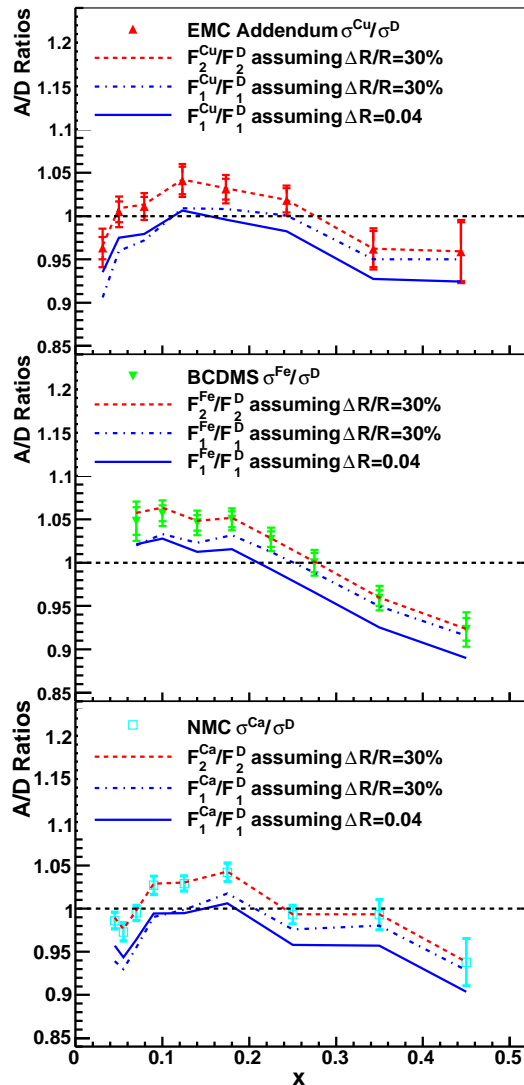


FIG. 4: The impact of the nontrivial nuclear dependence of  $R$  on the structure function ratios around the antishadowing region for BCDMS Fe/D [6], EMC Cu/D [8] and NMC Ca/D [10] data. The values of  $\epsilon$  are close to unity.

sumed in most phenomenological analyses.

### 3. EXPERIMENTAL LIMITS ON DETERMINING $R^A - R^D$

Thus far we have examined the impact of a nuclear dependence of  $R$  on the extraction of the nuclear dependent structure function ratios  $F_1^A/F_1^D$  and  $F_2^A/F_2^D$  from cross section ratios. The logical question then becomes: 'What is the limit on the experimental precision for  $R^A - R^D$ ?' In this section we shall explore this question within the context of the precision likely to be available for dedicated L/T separation measurements over the next decade or two. For guidance we shall refer to the highest pre-



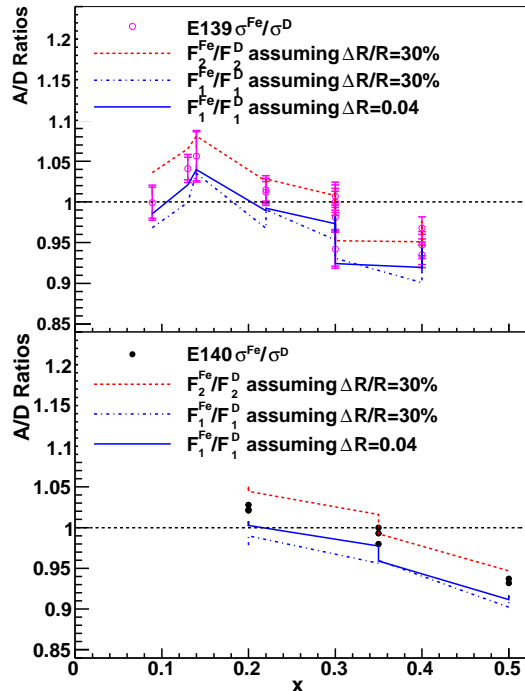


FIG. 5: The impact of the nontrivial nuclear dependence of  $R$  on the structure function ratios around the antishadowing region for SLAC E139 [7] and E140 [20] Fe/D data.

cision experiments performed at SLAC [7, 20, 23] and Jefferson Lab [21, 28]. These experiments have shown that reducing the  $\sigma_A/\sigma_D$  cross section ratio uncertainties, point-to-point in  $\epsilon$ , below 1% is experimentally challenging, yet obtainable. For instance, the point-to-point uncertainties from Jefferson Lab experiment E94110 [28] on cryogenic hydrogen have been estimated at about 1.5%, which was found to be consistent with the width of the distribution of residuals determined from the linear fits.

To measure cross sections at a range of  $\epsilon$  values for fixed  $x$  and  $Q$ , both the SLAC and JLab inclusive L/T separation experiments utilized a range of beam energies in conjunction with well studied spectrometer systems, which were able to be rotated to different angles and adjusted to accept varying ranges of momenta. Some of the largest contributions to the estimated systematic uncertainties stem from either time dependent systematics, such as current calibrations or detector efficiency variations, or from the uncertainties in the kinematics at each beam energy and spectrometer setting. However, these systematics largely cancel in the cross section ratios, in which the electron yields on each target are taken at the same kinematic settings and close in time.

If, for example, a 3% anti-shadowing effect in  $F_2^A$  were entirely due to a longitudinal enhancement, with  $F_1^A/F_1^D = 1$ , then this would be reflected in a 3% slope in the cross section ratio versus  $\epsilon' \equiv \epsilon/(1 + \epsilon R^D)$ , corresponding to  $\Delta R = R^A - R^D \approx 0.03$ . For the current study we assume the following:

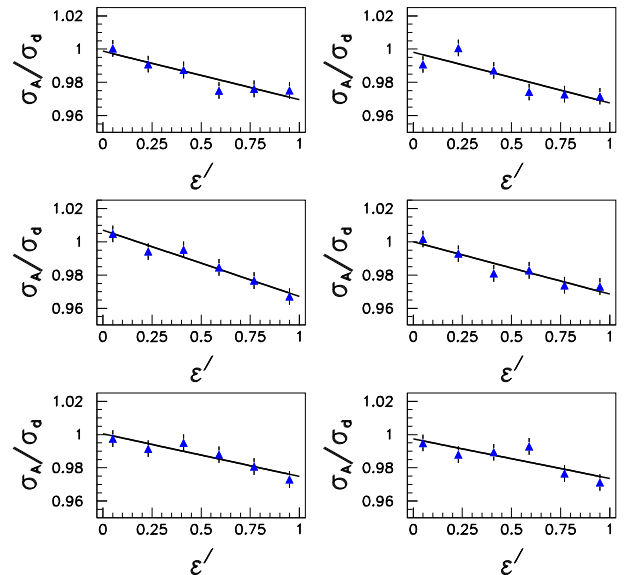


FIG. 6: Simulated  $\sigma^A/\sigma^D$  as a function of  $\epsilon'$  (data points with error bars) and a linear fit (solid lines), see the text for details.

- The total systematic point-to-point uncertainty (in  $\epsilon$ ) on the measured  $\sigma^A/\sigma^D$  ratios is 0.5%.
- There is no  $\epsilon$  dependent systematic uncertainty.
- Six cross section ratio measurements at equally spaced  $\epsilon' = \epsilon/(1 + \epsilon R^D)$  values in the range (0.05, 0.95), corresponding to six unique beam energies.

Under the assumptions above, the cross section ratios were selected at each  $\epsilon'$  by random sampling from a Gaussian distribution assuming a 3% slope on  $\sigma^A/\sigma^D$  versus  $\epsilon'$  and a Gaussian width of 0.5%. Six sample L/T separations generated by this procedure are shown in Fig. 6. After performing a linear fit, the uncertainty on the measured slope was found to be 0.67%, corresponding to a 1- $\sigma$  (3- $\sigma$ ) uncertainty on  $R^A - R^D$  of less than 0.007 (0.021). For the case considered of 0.5% ratio uncertainties, one could determine at 1- $\sigma$  whether a 3% antishadowing effect is due mainly to  $F_L^A$  to  $\approx 20\%$ .

We note that this uncertainty on the extracted  $R^A - R^D$  scales with the uncertainties on the cross section ratios such that a further reduction in the latter to 0.25% would reduce the uncertainty on  $\Delta R$  by half. However, we have thus far ignored any possible  $\epsilon$  dependent systematic uncertainties, such as those possibly arising from Coulomb and radiative corrections. For this reason, this is likely an optimistic scenario.

#### 4. NUCLEAR DEPENDENCE OF $R$ AND ITS ROLE IN ANTISHADOWING OF THE GLUON DISTRIBUTION IN NUCLEI

We demonstrated in Sect. 2.3 that the assumption of the nontrivial nuclear dependence of  $R$ , i.e.,  $R^A - R^D > 0$ , whose magnitude and sign are motivated by the NMC Sn/C data [26], leads to a difference between the cross section and structure function ratios:  $F_1^A/F_1^D < \sigma^A/\sigma^D < F_2^A/F_2^D$ . Moreover, the reduction of the  $F_1^A/F_1^D$  ratio is quite sizable: the enhancement in the  $0.1 < x < 0.3$  region visible in the cross section ratios is significantly decreased (or even disappears) for the  $F_1^A/F_1^D$  ratios, which indicates that antishadowing predominantly resides in the longitudinal structure function  $F_L^A$ . This conclusion is rather general; in particular, it does not rely on the twist expansion and the underlying partonic structure.

In the framework of the leading twist formalism, global QCD fits to the available data [13–17] show that the small enhancement of  $\sigma^A/\sigma^D$  in the antishadowing region translates into an enhancement of the valence quark and possibly gluon distributions in nuclei compared to those in the free proton. One should emphasize that these analyses assumed no nuclear dependence of  $R$ , i.e.,  $R = 0$ . The pattern and magnitude of nuclear modifications of the nuclear gluon distribution  $g_A(x)$  is known with very large uncertainty because  $g_A(x)$  is mostly determined indirectly from scaling violations of the nuclear structure function  $F_2^A$  measured in a limited kinematics. This is illustrated in Fig. 7 where we present the ratio of leading order gluon distributions in  $^{40}\text{Ca}$  to that in the free proton,  $g_A(x)/g_N(x)$ , as a function of  $x$  at fixed  $Q^2 = 3 \text{ GeV}^2$ . In the figure, the solid curve is the result of the EPS09 fit [16]; the dotted curve is the result of the HKN07 fit [15]; the dot-dashed curve is the nDS parameterization [14], whose results are quantitatively similar to those of [17]. For the EPS09 and HKN07 fits, we showed only the central values; the theoretical uncertainty on these predictions is quite large essentially in the entire range of  $x$ .

As one can see from Fig. 7, different groups predicts wildly different  $g_A(x)/g_N(x)$  (with large uncertainties). Since the amounts of nuclear shadowing and antishadowing are correlated through the momentum sum rule, large antishadowing corresponds to significant shadowing in the EPS09 fit [16]; very small antishadowing corresponds to negligibly small shadowing in the nDS fit [14]; the HKN07 fit [15] suggests yet another scenario where large gluon antishadowing is concentrated at large  $x$ .

Given the present uncertainty in  $g_A(x)$ , it is important and instructive to confront the NMC measurement of  $R^{Sn} - R^C$  [26] with direct calculations of this quantity in the framework of leading twist nuclear parton distributions. This is presented in Fig. 3 where the curves labeled “EPS09”, “HKN07” and “nDS” correspond to the direct calculation of  $R^{Sn} - R^C$  in the kinematics of the NMC measurement [26] using the respective leading

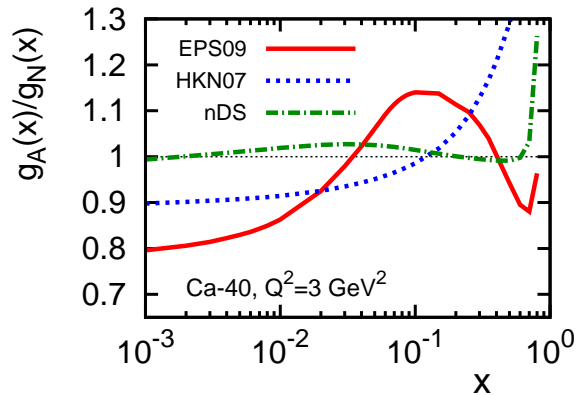


FIG. 7:  $g_A(x)/g_N(x)$  for  $^{40}\text{Ca}$  as a function of  $x$  at fixed  $Q^2 = 3 \text{ GeV}^2$  as obtained from global QCD fits. The solid (dotted, dot-dashed) curve is the result of the EPS09 [16] (HKN07 fit [15], nDS [14]) fit.

order parton distributions in nuclei. One can readily see from the figure that while for small  $x$ ,  $x < 0.05$ , the leading twist description is consistent with our assumptions for  $\Delta R \neq 0$  and the NMC data, in the antishadowing region  $0.1 < x < 0.3$  and also for larger  $x$  the leading twist approach predicts a negligibly small  $\Delta R$  in contrast with our assumptions and only marginally agrees with the data due to the large experimental uncertainty. Note that the leading twist calculations presented in Fig. 3 have rather small theoretical uncertainties stemming mostly from the uncertainty in the gluon distributions.

There are several reasons for the negligibly small value of  $R^{Sn} - R^C$  for  $x > 0.05$  at the NMC energies predicted in the leading twist framework. First and most importantly, the assumed shapes of the parameterizations of quark and gluon distribution in nuclei [14–17] are such that nuclear PDFs and the ratio  $R$  show only a weak nuclear dependence around  $x = 0.1$  (see Figs. 7 and 8). For instance, while the EPS09 analysis [16] used the data on  $Q^2$  dependence of  $F_2^{Sn}(x, Q^2)/F_2^C(x, Q^2)$  [26], it did not include the  $R^{Sn} - R^C$  data in the fit. Hence, resulting nuclear PDFs were not constrained to reproduce the experimental values of  $R^{Sn} - R^C$  which, as a result, leads to  $R^{Sn} - R^C \approx 0$  for  $x > 0.1$ . Second, while  $R^{Sn}/R^N$  and  $R^C/R^N$  separately reveal quite sizable deviations from unity (compare to  $R^{Ca}/R^N$  presented in the upper panel of Fig. 8), nuclear effects mostly cancel in the  $R^{Sn} - R^C$  difference. In general, while it is natural to expect  $\Delta R \neq 0$  because the pattern of nuclear modifications of quark and gluon distributions is different, with the currently assumed shapes of nuclear parton distributions it is not easy to generate sizable  $\Delta R$  for  $x > 0.1$  and large  $Q^2$  because  $R$  itself is very small there. Third, in the NMC kinematics the values of Bjorken  $x > 0.1$  correspond to  $Q^2 > 10 \text{ GeV}^2$ . At such large values of  $Q^2$ , nuclear modifications of parton distributions gradually become less pronounced. Note also that it is unlikely

that higher twist (twist-four) effects can generate sizable  $\Delta R$  because it would require unrealistically large higher twist effects [2].

While the available data on the nuclear dependence of  $R$  is not able to constrain the nuclear gluon distribution in the  $0.1 < x < 0.3$  region, a better chance of measuring gluon antishadowing would be offered by measurements of  $R$  with nuclear targets and the deuteron (proton) and at not too high  $Q^2$ . Note this is essentially equivalent to measuring the longitudinal structure functions  $F_L(x, Q^2)$  for nuclei and the deuteron (proton). Such measurements can be carried out at Jefferson Lab at 12 GeV at low-to-intermediate  $Q^2$  [29] and at a future Electron-Ion Collider (EIC) at intermediate-to-high  $Q^2$  [30, 31]. In the latter case, the measurement of  $F_2^A(x, Q^2)$  and the longitudinal nuclear structure function  $F_L^A(x, Q^2)$  (taking advantage of variable energies) with the subsequent extraction of  $g_A(x)$  in a wide kinematic range is already an important part of the planned physics program.

An example of expected nuclear effects is presented in Fig. 8 which shows predictions for the ratio of the nuclear to nucleon ratios  $R^A/R^N$  (upper panel) and longitudinal structure functions  $F_L^A/F_L^N$  (lower panel) as a function of  $x$  at  $Q^2 = 3 \text{ GeV}^2$  for  $^{40}\text{Ca}$ . Different curves correspond to different parameterizations of nuclear PDFs (see Fig. 7). A comparison of Figs. 7 and 8 shows that different assumptions about the shape of the gluon (and quark) distributions in nuclei lead to different shapes of  $R^A/R^N$  and  $F_L^A/F_L^N$ . To point out just one feature, an observation of sizable  $R^A/R^N > 1$  (enhanced  $F_L^A/F_L^N$  compared to  $F_1^A/F_1^N$ ) and  $F_L^A/F_L^N > 1$  in the antishadowing region  $0.1 < x < 0.3$  would unambiguously signal the presence of a significant antishadowing for the gluon distribution in nuclei. (The gluon distribution enters the longitudinal structure function  $F_L(x, Q^2)$  at the same order as the quark distributions; at the same time, the gluon distribution enters the transverse structure function  $F_1(x, Q^2)$  with the weight (coefficient function) that is smaller than that for  $F_2(x, Q^2)$  [32].) The converse is also true: an absence of nuclear enhancement of  $R^A/R^N$  and  $F_L^A/F_L^N$  in the interval  $0.1 < x < 0.3$  would translate into the absence of antishadowing for gluons in this region.

## 5. CONCLUSIONS

In this paper we studied the influence of the nontrivial nuclear dependence of  $R = \sigma_L/\sigma_T$  on the extraction of the  $F_2^A/F_2^D$  and  $F_1^A/F_1^D$  structure function ratios from the data on the  $\sigma^A/\sigma^D$  cross section ratios. Guided by indications of the nuclear dependence of  $R$  from the world data and, in particular, by the NMC measurement that showed that  $R^{S_n} - R^C = 0.040 \pm 0.021(\text{stat.}) \pm 0.026(\text{syst.})$  at  $\langle Q^2 \rangle = 10 \text{ GeV}^2$  [26], we tested two assumptions for  $\Delta R \equiv R^A - R^D$ :  $\Delta R = 0.04$  and  $\Delta R/R^N = 0.3$ , where  $R^N$  corresponds to the free proton [18]. With these assumptions, we examined se-

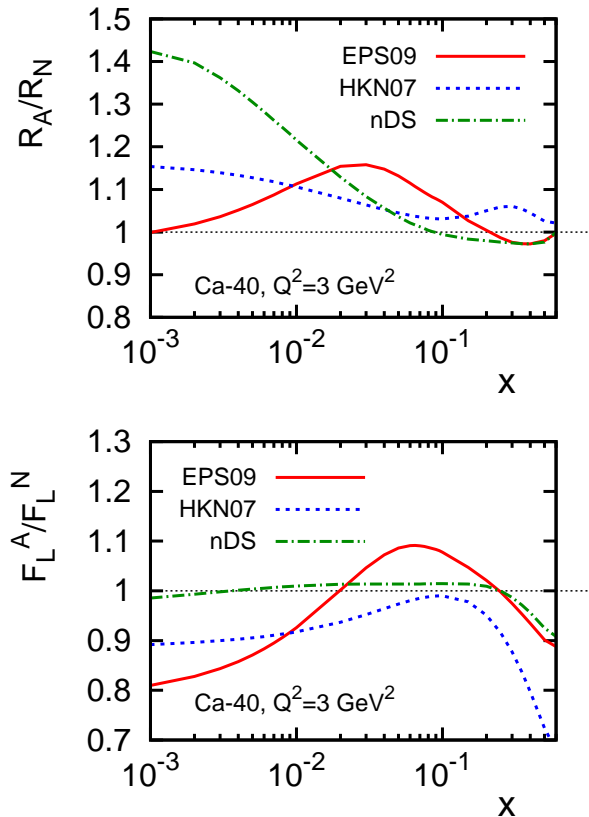


FIG. 8:  $R^A/R^N$  (upper panel) and  $F_L^A/F_L^N$  (lower panel)  $g_A(x)/g_N(x)$  for  $^{40}\text{Ca}$  as functions of  $x$  at  $Q^2 = 3 \text{ GeV}^2$ . The solid (dotted, dot-dashed) curve is the result of the EPS09 [16] (HKN07 fit [15], nDS [14]) fit.

lected sets of EMC, BCDMS, NMC and SLAC data on  $\sigma^A/\sigma^D$  and extracted the  $F_2^A/F_2^D$  and  $F_1^A/F_1^D$  ratios. We find that for the EMC, BCDMS and NMC data,  $F_2^A/F_2^D \approx \sigma^A/\sigma^D$ , while  $F_1^A/F_1^D < \sigma^A/\sigma^D$ . For the SLAC data, we found that  $F_1^A/F_1^D < \sigma^A/\sigma^D < F_2^A/F_2^D$ . In particular, we observed that the nuclear enhancement (antishadowing) in the interval  $0.1 < x < 0.3$  becomes significantly reduced (or even disappears in some cases) for the ratio of the transverse structure functions  $F_1^A/F_1^D$ . The latter observation indicates that antishadowing may in fact be dominated by the longitudinal contribution rather than by the transverse one (i.e., antishadowing is dominated by gluons rather than by quarks) as implicitly assumed by current phenomenological analyses and global nuclear parton distribution fits.

We also examined experimental limits on determining  $R^A - R^D$  from measurements of the  $\epsilon' = \epsilon/(1 + \epsilon R^D)$  dependence of  $\sigma^A/\sigma^D$ . Making a plausible assumption that  $\sigma^A/\sigma^D$  has a 3% slope in  $\epsilon'$  and can be measured with a 0.5% uncertainty over a broad range of  $\epsilon'$ , we found that  $\Delta R$  can be extracted with 0.67% uncertainty. Therefore, one could determine whether a 3% antishadowing effect is mainly due to  $F_L^A$  to approximately 20% accuracy.

In the leading twist framework, the magnitude of nu-



clear enhancement of  $R^A$  and the longitudinal structure function  $F_L^A(x, Q^2)$  (these quantities directly probe the nuclear gluon distribution  $g_A(x)$ ) is directly correlated with the size and shape of antishadowing for  $g_A(x)$ . While at the moment  $g_A(x)$  is rather poorly constrained by QCD fits to available data, a dedicated high-precision measurement of the nuclear dependence of  $R$  (the longitudinal nuclear structure function  $F_L^A(x, Q^2)$ ) at Jefferson Lab and an EIC has the potential to unambiguously constrain  $g_A(x)$  in the antishadowing region and beyond (An EIC will also be able to constrain  $g_A(x)$  deep in the shadowing region of small  $x$ .) Through the parton momentum sum rule, this knowledge will have a deep impact on  $g_A(x)$  in the entire range of  $x$ . In particular, it should dramatically help to constrain  $g_A(x)$  in the nu-

clear shadowing region,  $10^{-5} \leq x < 0.05$ , where  $g_A(x)$  plays an essential role in phenomenology of high-energy hard processes with nuclei, for a review, see [33].

### Acknowledgments

We are grateful to J. Gomez, W. Melnitchouk, P. Monaghan and M. Strikman for helpful discussions. This work was supported by the US Department of Energy contract No. DE-AC05-06OR23177, under which Jefferson Science Associates, LLC operates Jefferson Lab, and US National Science Foundation award No. 1002644.

- 
- [1] J. J. Aubert *et al.*[The European Muon Collaboration], Phys. Lett. B **123**, 275 (1983).  
 [2] L.L. Frankfurt and M.I. Strikman, Phys. Rept. **160**, 235 (1988).  
 [3] M. Arneodo, Phys. Rept. **240**, 301 (1994).  
 [4] D. F. Geesaman, K. Saito, and A. W. Thomas, Ann. Rev. Nucl. Part. Sci. **45**, 337 (1995).  
 [5] L. Frankfurt and M. Strikman, arXiv:1203.5278v1.  
 [6] A. C. Benvenuti *et al.*[The BCDMS Collaboration], Phys. Lett. B **189**, 483 (1987).  
 [7] J. Gomez *et al.*, Phys. Rev. D **49**, 4348 (1994).  
 [8] J. Ashman *et al.*[The European Muon Collaboration], Z. Phys. C **57**, 211 (1993).  
 [9] R. G. Arnold *et al.*, Phys. Rev. Lett. **52**, 727 (1984).  
 [10] P. Amaudruz *et al.*[The New Muon Collaboration], Nucl. Phys. B **441**, 3 (1995).  
 [11] K. Ackerstaff *et al.* [HERMES Collaboration], Phys. Lett. B **475**, 386 (2000) [Erratum-ibid. B **567**, 339 (2003)] [arXiv:hep-ex/9910071].  
 [12] D. M. Alde *et al.*, Phys. Rev. Lett. **64**, 2479 (1990).  
 [13] I. Schienbein *et al.*, Phys. Rev. D **77**, 054013 (2008); Phys. Rev. D **80**, 094004 (2009); K. Kovarik *et al.*, Phys. Rev. Lett. **106**, 122301 (2011).  
 [14] D. de Florian and R. Sassot, Phys. Rev. D **69**, 074028 (2004).  
 [15] M. Hirai, S. Kumano and T. H. Nagai, Phys. Rev. C **76**, 065207 (2007).  
 [16] K. J. Eskola, H. Paukkunen and C. A. Salgado, JHEP **0904** (2009) 065.  
 [17] D. de Florian, R. Sassot, P. Zurita and M. Stratmann, arXiv:1112.6324 [hep-ph].  
 [18] L. W. Whitlow *et al.*, Phys. Lett. B **250**, 193 (1990); L. W. Whitlow, Ph.D. Thesis, SLAC-REPROT-357, Stanford University (1990).  
 [19] K. Abe *et al.* [E143 Collaboration], Phys. Lett. B **452**, 194 (1999) [arXiv:hep-ex/9808028].  
 [20] S. Dasu *et al.*, Phys. Rev. D **49**, 5641 (1994).  
 [21] V. Tvaskis *et al.*, Phys. Rev. Lett. **98**, 142301 (2007); V. Tvaskis, Ph.D Thesis, *Longitudinal-Transverse Separation of Deep-Inelastic Scattering at low  $Q^2$  on Nucleons and Nuclei*, Vrije Universiteit (2004).  
 [22] M. Arneodo *et al.*[The New Muon Collaboration], Nucl. Phys. B **487**, 3 (1997).  
 [23] L. H. Tao *et al.*, Z. Phys. C **70**, 387 (1996).  
 [24] P. Solvignon, D. Gaskell and J. Arrington, AIP Conf. Proc. **1160**, 155 (2009) [arXiv:0906.0512 [nucl-ex]].  
 [25] P. Amaudruz *et al.* [New Muon Collaboration], Phys. Lett. B **294**, 120 (1992).  
 [26] M. Arneodo *et al.*[The New Muon Collaboration], Nucl. Phys. B **481**, 23 (1996).  
 [27] S. Dasu *et al.*, Phys. Rev. Lett. **60**, 2591 (1988).  
 [28] M. E. Christy *et al.* [E94110 Collaboration], Phys. Rev. C **70**, 015206 (2004).  
 [29] JLab 12 GeV proposal PR12-11-113, spokespersons: L. Y. Zhu, M. E. Christy, C. E. Keppel, D. Gaskell, and P. Solvignon, *Detailed Studies of the Nuclear Dependence of  $R = \sigma_L/\sigma_T$* .  
 [30] D. Boer *et al.*, arXiv:1108.1713 [nucl-th].  
 [31] A. Accardi, V. Guzey, A. Prokudin and C. Weiss, Eur. Phys. J. A **48**, 92 (2012) [arXiv:1110.1031 [hep-ph]].  
 [32] R. Brock *et al.* [CTEQ Collaboration], Rev. Mod. Phys. **67**, 157 (1995).  
 [33] L. Frankfurt, V. Guzey and M. Strikman, Phys. Rept. **512**, 255 (2012) [arXiv:1106.2091 [hep-ph]].